

# Module-Wise Network Quantization for 6D Object Pose Estimation

Saqib Javed<sup>1</sup>

Andrew Price<sup>2</sup>

Yinlin Hu<sup>3</sup>

Mathieu Salzmann<sup>1,4</sup>

<sup>1</sup> CVLab, EPFL

<sup>2</sup> Space Robotics Lab, Tohoku University

<sup>3</sup> MagicLeap

<sup>4</sup> ClearSpace SA

## Abstract

Many edge applications, such as collaborative robotics and spacecraft rendezvous, can benefit from 6D object pose estimation, but must do so on embedded platforms. Unfortunately, existing 6D pose estimation networks are typically too large for deployment in such situations and must therefore be compressed, while maintaining reliable performance. In this work, we present an approach to doing so by quantizing such networks. More precisely, we introduce a module-wise quantization strategy that, in contrast to uniform and mixed-precision quantization, accounts for the modular structure of typical 6D pose estimation frameworks. We demonstrate that uniquely compressing these modules outperforms uniform and mixed-precision quantization techniques. Moreover, our experiments evidence that module-wise quantization can lead to a significant accuracy boost. We showcase the generality of our approach using different datasets, quantization methodologies, and network architectures, including the recent ZebraPose.

## 1. Introduction

Efficient, reliable and accurate 6D pose estimation is a core competency of many computer vision tasks. In particular, it plays a critical role in many robotics applications, such as automated manufacturing [31], vision based control [35], collaborative robotics [42] and spacecraft rendezvous [37]. However, such applications come with their own challenges: They must typically run on embedded platforms, and thus with limited hardware resources.

These resource constraints largely disqualify the recent state-of-the-art methods, such as ZebraPose [38], SO-Pose [9], GDRNet [43], which employ a two stage approach (detection followed by pose estimation) and thus entail a large memory footprint. In this context, single-stage methods [6, 15, 18, 30, 34, 36, 41, 44] offer a more pragmatic alternative, yielding models with a good accuracy-footprint tradeoff. Nevertheless, these models remain too large for deployment on edge devices.

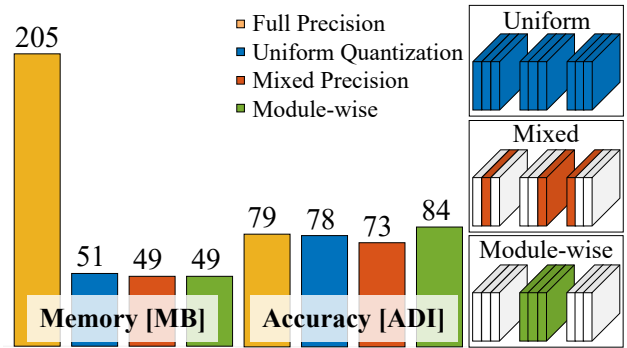


Figure 1. **Summary of this Work.** In contrast with uniform and mixed-precision quantization, our module-wise quantization strategy accounts for the modular structure of typical 6D object pose estimation frameworks. We demonstrate that this not only reduces the memory footprint of the network but may come with an accuracy boost that neither uniform nor mixed-precision quantization have witnessed.

CA-SpaceNet [44] addresses this by further quantizing the network to reduce the memory footprint. However, this is achieved using a uniform quantization approach wherein all network layers are quantized to the same bit width, except for the first and last layer. This precludes the use of aggressive quantization (i.e., two bits), which would incur large accuracy losses. In principle, this could be alleviated by using mixed-precision quantization [5, 10, 39]. However, these techniques target individual layers, and determining the optimal bit precision for each layer is complex, requiring intricate post training network search algorithms or hundreds of GPU hours.

In this work, we propose to exploit the modular structure of 6D pose estimation frameworks to make better use of quantization. Indeed, typical state-of-the-art 6D pose estimation networks are composed of multiple modules, such as backbone, decoder, and head. Here, we evidence that each module demonstrates varying sensitivity to quantization and consequently argue that they should be quantized differently. In particular, our extensive ablation studies show that aggressively quantizing (i.e., 2 bit quantization)

certain modules can yield a significant accuracy boost over the original full-precision network. In other words, and as summarized in Figure 1, this lets us obtain a network that outperforms alternatively quantized networks in both inference accuracy and memory storage metrics, simultaneously.

Our contributions can be summarized as follows:

- We propose to exploit the modular structure of 6D pose estimation for targeted network quantization.
- We explore the sensitivity to quantization of different single-stage pose estimation modules.
- In particular, we show that aggressive quantization of Feature Pyramid Network (FPN) modules can greatly **improve** the accuracy of state-of-the-art single-stage 6D pose estimation methods.

We demonstrate the generality of our approach by applying it to different single-stage architectures, WDR [18], CA-SpaceNet [44]; different datasets, SwissCube [18], Linemod [14], and Occlusion Linemod [3]; and using different quantization strategies, INQ [50] and LSQ [12]. We further show that our method also applies to two-stage networks, such as the state-of-the-art ZebraPose [38], on which it outperforms uniform and mixed-precision quantization.

## 2. Related Work

We first present and broadly categorize relevant RGB-based 6D pose estimation architectures. We then discuss recent quantization methods applicable to pose estimation network architectures.

### 2.1. 6D Pose Estimation

*Single-Stage Direct Estimation.* PoseCNN [45] was one of the first to estimate 6D object pose using a deep neural network. The network comprised a backbone feature extractor which fed into three heads: a labeller, a segmenter and a fully-connected head to regress the pose directly. Unfortunately, representing the  $SO(3)$  group rotations in a manner suitable for direct regression can prove challenging. SSD6D [21, 26] instead proposed a discretization of the rotation space to form a classification problem instead of a regression one. URSONet [33], and more recently Mobile-URSONet [32], demonstrated competitive results via a backbone–bottleneck–head structure to estimate the weights of a set of “classification” quaternions corresponding to Euler angle rotations.

*Single-Stage with PnP.* In general, a better performing strategy is to have a network trained to predict 2D correspondences instead of the pose. The pose is then obtained via a RANdom SAMple Consensus (RANSAC) / Perspective-n-Point (PnP) 2D-to-3D correspondence fitting process. These methods typically employ a backbone,

a feature decoder and one or multiple heads [6, 17–20, 29, 30, 34, 40, 41, 44, 48]. [34, 40] estimate these correspondences in a single global fashion, while [17, 20, 29, 30, 48] aggregate multiple local predictions to improve robustness. To improve 2D correspondence prediction performance in the presence of large depth variations, a number of works [18, 41, 44] use an FPN [25] to exploit features at different scales.

*Multi-Stage with PnP.* The current state-of-the-art pose estimation frameworks incorporate a pipeline of networks to perform different tasks [9, 22, 24, 38, 43]. In the first stage network, the target is localized and a Region of Interest (RoI) is cropped and forwarded to the second stage network. This isolates the position estimation task from the orientation estimation task and further provides the orientation estimation network with an RoI containing only object features. The second stage orientation estimation network can then more easily fit to the target object. Therefore, these multi-stage frameworks tend to yield more accurate results but also much larger memory footprints as they may include one object classifier network; one object position/RoI network; and  $N$  object pose networks.

For hardware-restricted 6D pose estimation cases, a multi-stage framework may not be practical. Even for single-stage networks, additional compression [2] is required. Next, we discuss achieving network compression via quantization.

### 2.2. Quantization

Quantizing a neural network refers to the process of reducing the numerical precision of the network parameters, weights and activations. Existing methods can be grouped into post training quantization [4, 13, 23, 27, 28, 49], uniform Quantization Aware Training (QAT) [1, 12, 46, 50], and mixed precision QAT [5, 7, 10, 11, 39, 47].

*Post-training* methods are more restricted as they cannot fine-tune the model as the weights change. The methods that follow this strategy use only a small number of unlabeled samples to calibrate the activations’ dynamic range. The use of a small subset (often 1024 samples) of training samples helps to avoid overfitting. Recent methods [13, 23, 27] perform layer-by-layer or block-by-block optimization to minimize the error between the quantized layer/block output and the full-precision layer/block output.

*Uniform QAT* methods treat each layer of the network uniformly during quantization. Incremental Network Quantization (INQ) [50] selects a bit precision and quantizes a fraction of the network at a time. A uniform fraction of each layers’ weights are then quantized and training continues until the next quantization step. Quantization can be achieved in a structured manner, where entire kernels are quantized at once, or in an unstructured manner. In contrast to INQ, Learned Step-size Quantization (LSQ) [12] quan-

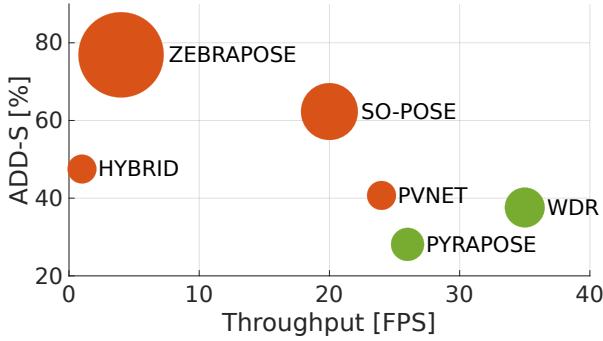


Figure 2. **Performance Comparison on O-LINEMOD.** Methods training individual models for each object are shown in orange. Methods training a single model for all objects are shown in green. The marker size is proportional to the memory footprint.

tizes the entire network in a single action. To this end, LSQ treats the quantization step-size as a learnable parameter. The method then alternates between updating the weights and the step-size parameter.

*Mixed-precision QAT* methods, conversely, treat each network layer uniquely, aiming to determine the appropriate bit precision for each layer. In HAWQ [10, 11, 47], the network weights’ Hessian is leveraged to assign bit precisions proportional to the gradients. In [5], the mixed precision is taken even further by applying a different precision to different kernels within a single channel. While promising, mixed-precision QAT is a challenging task, and existing methods remain computationally expensive for modern deep network architectures.

*Quantization for 6D Pose Estimation.* To the best of our knowledge, only CA-SpaceNet [44] has exploited quantization for 6D pose estimation, simply using an existing uniform quantization method. Note that none of the quantization methods discussed above adapt to or acknowledge the intended task or the network architecture. By contrast, we argue that, as different components of a network are optimized to perform different tasks, these components should also be quantized differently. We evidence this by exploiting the modular structure of 6D pose estimation networks.

### 3. Method

Let us now introduce our approach to exploiting the structure of 6D pose estimation networks during quantization. Below, we first describe the general type of network architecture we consider for compression and then introduce our module-wise quantization methodology.

#### 3.1. Network Architecture

As discussed in Section 2, multi-stage networks [9, 22, 24, 38, 43] tend to induce large memory footprints and large latencies, thus making poor candidates for hardware-

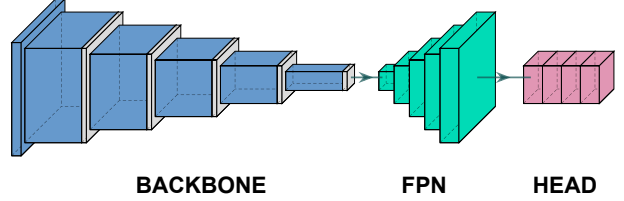


Figure 3. **Representative Single-Stage 6D Pose Estimation Network with  $K = 3$  modules.**

restricted applications. This is further evidenced in Figure 2, which compares a number of 6D pose estimation architectures’ memory footprint, throughput and accuracy on the O-LINEMOD dataset. While demonstrating admirable accuracy, the size and latency of ZebraPose [38] and SO-Pose [9] preclude their inclusion in hardware-restricted platforms.

On this basis, we therefore focus on single-stage 6D pose estimation networks [18, 30, 40, 41, 44].<sup>1</sup> In general, such networks consist of multiple modules, exhibiting an encoder-decoder structure followed by prediction heads. A commonly used structure that has proven effective in practice, particularly to handle large object scale variations, relies on  $K = 3$  basic modules,  $\{B_1, B_2, B_3\}$ , corresponding to the feature extraction backbone, an FPN and prediction heads (which we consider as a single module), respectively. Examples of such a structure include PyraPose [41], WDR [18], and CA-SpaceNet [44]; a representative generic architecture is illustrated in Figure 3. Below, we explain how we exploit this modular structure for quantization.

#### 3.2. Module-Wise Quantization (MQ)

Traditional Quantization Aware Training (QAT) methods [1, 12, 46, 50] treat each layer of the network uniformly during quantization. While this effectively reduces the network’s memory footprint, it tends to degrade its performance as quantization becomes increasingly aggressive, such as with ternary weights  $\{-1, 0, 1\}$ . Here, instead, we propose to exploit the modular structure of 6D pose estimation networks to quantize each module differently, resulting in a non-uniform quantization strategy. As shown below, our **Module-wise Quantization (MQ)** strategy requires minimal effort to implement compared to a layer-wise or mixed precision quantization method [5, 8, 10, 11, 39, 47].

Specifically, module-wise quantization begins by performing aggressive quantization (i.e., ternary weights) with a modified uniform QAT method (e.g., INQ [50], LSQ [12]) on a single module of the network. This process is repeated for all  $K$  modules, where, at each step, only the  $k^{th}$  module is quantized while the remaining  $K - 1$  modules retain full

<sup>1</sup>For completeness, we also demonstrate that our quantization approach applies to two-stage networks (e.g. ZebraPose [38]).

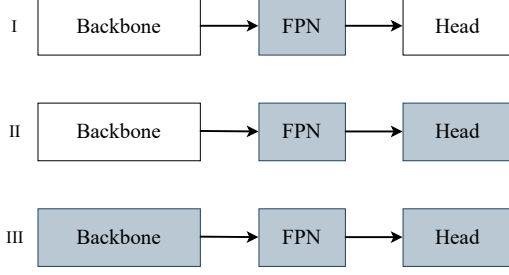


Figure 4. **Example Quantization Flow for a 6D Pose Estimation Network.** This corresponds to first quantizing the FPN, then the head, and finally the backbone.

precision. The quantization of only a selected module  $B_k$  provides flexibility for the other  $K - 1$  full precision modules to compensate for any accuracy loss; in some cases *accuracy can even improve* as will be shown in Section 4.

The strategy described above considers each separate module at a time. To quantize the entire network in a module-wise fashion, we proceed as follows. Given the results of the aggressive quantization of each individual block, we define a quantization flow, which determines in what order the modules should be quantized. We then sequentially quantize the modules in this order, determining the optimal bit precision for each module. The resulting module-wise quantization strategy is provided in Algorithm 1 and described in more detail below. The results of MQ in conjunction with LSQ and INQ will be demonstrated in Section 4. Note that any traditional QAT algorithm can be applied as input,  $Q$ , in lieu of INQ or LSQ.

### 3.2.1 MQ Algorithm

**Sensitivity Search** (Lines 10:16). For a network with  $K$  modules,  $K$  independent 2 bit quantizations are performed. If the quantized module,  $B_k^q$ , increases the accuracy of that network,  $M_k^q$ , we keep that model and the current index  $k$ . Note that the results of this initial sensitivity search can be used to infer a suitable bit precision schedule,  $q$ , and a feasible accuracy threshold,  $\tau$  (i.e., some networks can better accommodate aggressive quantization and thus allow for a higher  $\tau$ ).

**Quantization Flow** (Lines 17:23). Sequentially quantizing the modules of a network is not commutative. Therefore, the order of module quantization must be chosen with care. First, if an accuracy gain is observed when quantizing module  $B_k$ , it is best to start from the corresponding network,  $M_k^q$ ; accuracy losses will not be recovered in the subsequent quantization steps. If no accuracy gain is obtained, proceed with quantizing the module with the lowest number of parameters first. The modules with higher parameter numbers will have more flexibility to adapt to aggressive quantization. The resulting *flow* list is passed to the next

---

#### Algorithm 1 Module-wise Quantization (MQ)

---

```

1: Input: Training data,
2: Input: QAT method  $Q$ 
3: Input: Model  $M$ , with modules  $\mathbf{B} = [B_1, B_2, \dots, B_K]$ 
4: Input: Model accuracy metric  $ac(M)$ 
5: Input: Accuracy threshold  $\tau$ 
6: Input: Bit-width search  $q = [2, 4, 6 \dots]$ 

7:  $flow = []$ ,
8:  $ac(M_{best}) \leftarrow 0$ ,
9:  $k_{best} \leftarrow 0$ ,
10:  $i \leftarrow 0$ 
11: for  $k = 1, 2, \dots, K$  do
12:    $M_k^2 \leftarrow Q_k^2(M)$ 
13:   if  $ac(M_k^2) > ac(M) \wedge ac(M_k^2) > ac(M_{best})$  then
14:      $M_{best}^2 \leftarrow M_k^2$ 
15:      $k_{best} \leftarrow k$ 
16:   end if
17: end for
18: if  $M_{best}$  then
19:    $M \leftarrow M_{best}$ 
20:    $flow \leftarrow index(SORT\_SIZE(\mathbf{B}))$ 
21:    $flow.pop(k_{best})$ 
22: else
23:    $flow \leftarrow index(SORT\_SIZE(\mathbf{B}))$ 
24: end if
25: while  $i \leq len(flow)$  do
26:    $M^Q \leftarrow Q_{flow(i)}^q(M)$ 
27:   if  $(ac(M^Q) > \tau)$  then
28:      $i \leftarrow i + 1$ 
29:      $M \leftarrow M^Q$ 
30:   else
31:      $q \leftarrow q + 1$ 
32:   end if
33: end while
34: Output: Optimized bit-width quantized model ( $M^Q$ )
    that meets the application accuracy threshold.
```

---

- $K$ : Number of modules
  - $M_k^q$ : Model with only module  $k$  quantized to  $q$  bits.
  - $flow$ : Sequence of quantization order of modules.
  - $M^Q$ : Model with several modules quantized to diff. bit precisions.
  - $Q_c^j$ : Quantization applied to module  $B_c$  with  $j$ -bits.
  - $k_{best}$ : Index of the module for which quantization increased perf.
-



section. It indicates the order of module quantization as exemplified in Figure 4.

**Optimal Bit Precision** (Lines 24:32). Finally an optimal bit precision search is performed in the order specified by *flow*. Using the bit-width search schedule input on line 4, we begin with aggressive quantization of module  $B_{k=flow(i)}$  into model  $M^Q$ . If the accuracy meets the accuracy threshold,  $\tau$ , we proceed to the next module indicated by *flow*. If the accuracy does not meet the accuracy threshold,  $\tau$ , we increase the quantization bit precision according to the schedule,  $q$ , and repeat.

Finally, MQ outputs the maximally-compressed model  $M^Q$  that meets the accuracy threshold,  $\tau$ .

Historically, quantization and other compression methods have been used to exercise a trade-off between inference accuracy and feasibility of deployment, particularly in resource-constrained circumstances. In the following sections, we will show that our approach may yield a significant inference accuracy improvement. To the best of our knowledge, this is the first time quantization has demonstrated such a consistent enhancement; this result may warrant further exploration. Furthermore, we will show that our method generalizes to different datasets, network architectures, and quantization methods.

## 4. Experiments

In this section, we first introduce the datasets and metrics used for evaluation. Next, we present ablation study experiments to explore the nature of MQ enhancing network accuracy; this result is directly compared to uniform and mixed QAT methods. Finally, we demonstrate the generality of our method applied to different datasets, network architectures, and QAT methods.

### 4.1. Implementation Details

We use PyTorch for the implementation of our experiments. For the retraining of our partially quantized pre-trained network, we employ an SGD optimizer with a base learning rate of  $1e^{-2}$ . We use a batch size of 8 and 30 epochs for all of our experiments, and a hand-crafted learning scheduler which decreases the learning rate at regular intervals by a factor of 10 and increases it again when we quantize a module with INQ [50]. However, when we quantize our modules using LSQ [12], the learning rate factor is not increased, only decreased by factors of 10. We use 512x512 resolution input for the SwissCube dataset and 640x480 for LINEMOD and O-LINEMOD as in [30].

#### 4.1.1 Datasets and Metrics

Historically, LINEMOD and O-LINEMOD have been the most widely used datasets to benchmark 6D pose estimation methods. The LINEMOD dataset contains 13 different

sequences, each of which consists of ground-truth poses for a single object of interest in a cluttered environment. CAD models are also provided for each object. We follow the settings of PVNet [30] and GDRNet [43] and utilize 15% of the images for training and the remaining 85% for testing. O-LINEMOD extends LINEMOD into a more challenging dataset by including occlusions on 8 objects. The testing data contains only 1214 images with severe occlusions. For both datasets, additional rendered images are used during training [9, 18, 30, 38, 43]. Similarly to previous works, we use the ADD error metric [16] expressed as

$$e_{ADD}(P^{est}, P^{gt}) = \frac{1}{V} \sum_{i=1}^V \|P_i^{est} - P_i^{gt}\|_2, \quad (1)$$

where  $P_i^{est}$  and  $P_i^{gt}$  denote the  $i^{th}$  vertex of the 3D mesh model after transformation with the predicted and ground-truth pose, respectively. We then report the accuracy using the “ADD-0.1d” and “ADD-0.5d” metrics, which encode the proportion of samples for which  $e_{ADD}$  is less than 10% and 50% of the object diameter, respectively.

While challenging in themselves, the LINEMOD and O-LINEMOD datasets are limited in scope to household items, with stable uniform lighting and no large depth variations. Conversely, the SwissCube dataset [18] embodies a challenging scenario for 6D pose estimation in space, incorporating large scale variations, diverse lighting conditions and variable backgrounds. It consists of 500 synthetic sequences, each with 100 images. Of the 50k images, we used 40K for training, and the remaining 10K for testing, as in [18] and [44]. To remain consistent with previous works evaluating on SwissCube, the ADI metric [16] is used.<sup>2</sup> It is computed as

$$e_{ADI}(P^{est}, P^{gt}) = \frac{1}{V} \sum_{i=1}^V \min_{j \in [1, V]} \|P_i^{est} - P_j^{gt}\|_2. \quad (2)$$

Similarly to the ADD case, we report the “ADI-0.1d” and “ADI-0.5d” metrics to evaluate accuracy on the Swisscube dataset. The robustness of MQ for 6D pose estimation frameworks is thus demonstrated on diverse datasets.

### 4.2. Quantization Study

Let us now study the behavior of MQ in detail and show that it outperforms traditional QAT methods. All experiments in this section were made on the SwissCube dataset.

<sup>2</sup>As discussed in [16], the ADI metric was proposed for image sets with *indistinguishable* poses, e.g., symmetric objects. ADI is in fact a lower bound of ADD and is therefore a more permissive metric. While it can be argued that ADD would also be a more suitable metric for the SwissCube dataset, ADI is used here so as to compare fairly with previous works.

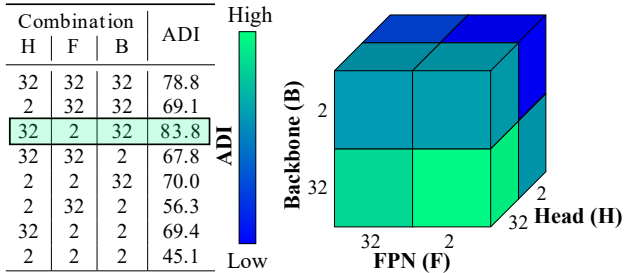


Figure 5. MQ Bit Precision Sensitivity Search.

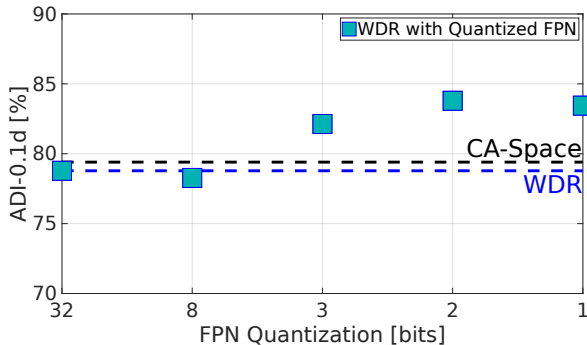


Figure 6. Effect of FPN Quantization on Accuracy.

#### 4.2.1 MQ Ablation Study

We first perform an ablation study to validate the optimal order for quantizing the network modules. As discussed in Section 3.2.1, the module quantization order is not commutative. Using WDR, we perform aggressive quantization to every combination of modules in the network. This is an  $O(2^K)$  search; this results in eight module quantization combinations for a network with  $K = 3$  modules. The results are visualized in Figure 5. The backbone and head modules exhibit greater sensitivity to aggressive quantization. Conversely, the accuracy of the network is enhanced when using 2 bit quantization on the FPN module only. No other combination of module quantizations yields an accuracy increase. This further emphasizes the importance of carefully selecting a module quantization flow. Note that extending this study by quantizing more modules simultaneously simply converges to a uniform QAT method. A potential follow up would be to apply MQ to architectures with even more modules or to instead classify large modules as two or more modules for the purposes of MQ.

We additionally perform ablation studies on the optimal order (i.e., flow) of module quantization. We begin by quantizing different modules first, instead of the FPN. Table 1 shows the results of both the head and backbone modules when they are the first module quantized. We observe that the inference accuracy decreases dramatically for both cases. No combination of module flow or bit precision

Network (First Quantized Module)	ADI	
	0.1d	0.5d
Full Precision	78.79	98.98
Backbone	69.08	96.79
Head	67.84	98.12
FPN	<b>83.9</b>	<b>99.4</b>

Table 1. Effect of Quantizing Different Modules First.

sion schedule is able to recover the inference accuracy after it was lost. The 2 bit aggressive FPN quantization yields improved accuracy only when the FPN is quantized first.

#### 4.2.2 Quantized FPN Sensitivity Study

To expand upon the 2 bit FPN accuracy enhancement, we perform a higher granularity bit-precision search on the FPN module. Again, the FPN module was quantized, but to five different bit-widths for comparison; the results are presented in Figure 6. The accuracy of two full-precision networks, WDR [18] and CA-SpaceNet [44], are shown with dashed lines. The highest accuracy is achieved with a 2 bit or ternary  $\{-1, 0, 1\}$  FPN. Further pushing the FPN to binary weights  $\{-1, 1\}$  slightly reduces the accuracy, but maintains a significant improvement over both baselines.

Layer	Near	Medium	Far	All
1	13.6 (+0.8)	83.8 (+1.0)	55.1 (+6.2)	52.9(+3.0)
2	13.6 (+2.6)	83.8 (+1.3)	55.1 (+0.3)	54.1 (+1.3)
3	16.3 (-0.5)	77.8 (+1.6)	17.1 (-1.2)	37.2 (-0.1)
4	13.0 (+0.7)	0.41 (+0.7)	0 (0)	3.8 (+0.4)

Table 2. Layer-wise 6D Pose Validation Results with a Quantized FPN. We report the full precision ADI-0.1d, with the improvement due to 2 bit quantization in parentheses.

Delving further, the FPN layer-wise ADI-0.1d inference accuracies are shared in Table 2. With the exception of layer 3, it can be seen that aggressive quantization improves the performance of every layer at every scale. While improvement is observed at every depth range, an especially large performance enhancement is observed at layer 1 for *Far* objects. In essence, the 2 bit quantization of the FPN acts as a regularizer; with a lower precision and the relatively low number of parameters in the FPN, the layers cannot easily overfit to the train data.

#### 4.2.3 MQ Compared to Uniform and Mixed QAT

Historically, QAT methods do not significantly enhance network inference accuracy, and we demonstrate this again here. In a typical hardware-limited application, a suitable

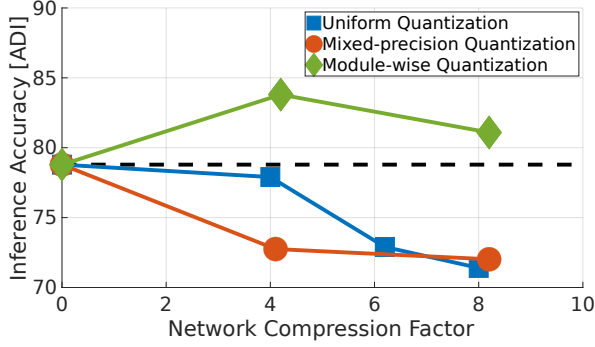


Figure 7. Uniform QAT vs Mixed QAT vs MQ.

Bit Precision	ADI-0.1d	ADI-0.5d	Compression
FP32	78.8	98.9	0
INQ 8 bits	77.9	98.8	4x
HAWQv3	72.1	98.1	4.2x
<b>MQ (ours)</b>	<b>83.8</b>	<b>99.4</b>	4.2x
INQ 5 bits	72.9	98.6	6.4x
INQ 4 bits	71.4	98.5	8.0x
HAWQv3	71.7	98.7	8.2x
<b>MQ (ours)</b>	<b>81.1</b>	<b>99.1</b>	8.2x

Table 3. Uniform QAT vs MQ. We report ADI scores on the SwissCube dataset for various compression factors. The entries are sorted by compression factor.

network is selected and then compressed to meet the hardware constraints. For direct comparison, we apply three different quantization paradigms. Starting from a full precision WDR network, we apply a uniform QAT method, INQ [50], a mixed-precision QAT method, HAWQv3 [47], and finally our proposed MQ method with increasing compression factors. The results are provided in Figure 7 and Table 3. Again, MQ demonstrates a significant accuracy improvement while sustaining the requested compression factor; it is the only quantization approach to show an increase in inference accuracy during compression.

### 4.3. MQ Generality

Finally, we demonstrate the generality of MQ to different datasets, different QAT methods and different architectures.

#### 4.3.1 Dataset and QAT Generality

As discussed in Section 4.1.1, the image domains of LINEMOD, O-LINEMOD and SwissCube are vastly different. The full precision and 2 bit quantized FPN results for all three datasets are shown in Table 4. MQ demonstrates an accuracy improvement in all datasets. We use the ADI metric for evaluation on the SwissCube dataset as in [18, 44], while we use the ADD metric for LINEMOD

Quantization Mode	Swisscube		Linemod		Occ. Linemod	
	0.1d	0.5d	0.1d	0.5d	0.1d	0.5d
Full precision	78.8	98.9	56.1	99.1	37.8	85.2
Quantized FPN <sub>LSQ</sub>	83.4	99.3	63.6	99.2	39.8	86.4
Quantized FPN <sub>INQ</sub>	<b>83.8</b>	<b>99.4</b>	<b>63.9</b>	<b>99.5</b>	<b>40.2</b>	<b>86.7</b>

Table 4. Quantized FPN in WDR network on different datasets. Following common practice, we report ADI scores for Swisscube and ADD ones for both LINEMOD and O-LINEMOD.

Network	Near	Medium	Far	All
SegDriven-Z [17]	41.1	22.9	7.1	21.8
DLR [6]	52.6	45.4	29.4	43.2
CA-SpaceNet	91.0	86.3	61.7	79.4
CA-SpaceNet*	95.5	90.7	66.2	82.7
WDR	92.4	84.2	61.3	78.8
WDR*	<b>96.1</b>	<b>91.5</b>	<b>68.2</b>	<b>83.8</b>

Table 5. Comparison with the state-of-the-art on SwissCube. We report ADI-0.1d scores for 3 different depth ranges. A \* indicates a MQ 2 bit FPN model.

and O-LINEMOD as used by [22, 30, 38, 41, 43].

Accuracy improvements of 5.0%, 7.8% and 2.4% are demonstrated on SwissCube, LINEMOD and O-LINEMOD, respectively, when MQ with INQ is utilized. Replacing INQ with LSQ yields accuracy improvements of 4.6%, 7.5% and 2.0%, respectively. This evidences that the performance enhancement is independent of the dataset domain and the applied QAT method.

As discussed in Section 3.2.1 and Section 4.2.1, it is difficult to recover accuracy once it is lost during quantization. To this end, since INQ [50] quantizes only a fraction of the network at once, it follows that the remaining unquantized portion of the network is left flexible to adapt to aggressive quantization. Conversely, LSQ [12] quantizes the entire network in a single step; no fraction of the network is left unperturbed. Consequently, INQ demonstrates superior results in Table 4. While any QAT method may be used, we recommend partnering MQ with INQ for optimal aggressive quantization results.

#### 4.3.2 Architecture Generality

In Table 5, we compare several single-stage PnP architectures on the SwissCube dataset. To demonstrate the generality of our performance enhancement, we aggressively quantize the FPN of both CA-SpaceNet [44] and WDR [18]. We demonstrate an accuracy improvement of 4.5%, 4.4% and 4.5% for Near, Medium and Far images, respectively, on CA-SpaceNet, resulting in a total testing set accuracy

Quantization Mode	ADI-0.1d	Compression
CA-SpaceNet	79.4	1x
8 bit CA-SpaceNet B	76.2	2.2x
8 bit CA-SpaceNet BF	75.0	3.2x
8 bit CA-SpaceNet BFH	74.7	4.0x
<b>CA-Space MQ (Ours)</b>	<b>82.7</b>	4.7x
3 bit CA-SpaceNet B	75.1	2.9x
3 bit CA-SpaceNet BF	74.5	5.9x
<b>CA-SpaceNet MQ (Ours)</b>	<b>80.2</b>	8.2x
3 bit CA-SpaceNet BFH	68.7	10.6x

Table 6. **CA-SpaceNet Published Quantization vs MQ**. We report ADI scores on the SwissCube dataset with different compression factors. The entries are sorted by compression factor.

improvement of 3.3%. Recall the already presented total testing set accuracy improvement of 5.0% for WDR. Previously, the full precision CA-SpaceNet had shown a performance improvement over the full precision WDR, but WDR sees greater gains from the application of MQ.

In addition, [44] published accuracy results for a uniform QAT quantized CA-Space network, shared in Table 6. Specifically, CA-SpaceNet explored three quantization “modes”. “B” corresponds to only quantizing the backbone; “BF” corresponds to quantizing the backbone and FPN (paired); and “BFH” corresponds to quantizing the whole network (uniformly). As we demonstrated in Section 4.2.1, quantizing network modules in pairs greatly reduces inference accuracy as the smaller unquantized fraction of the network is not able to adapt to the quantization. Additionally, quantizing from backbone to head does not consider the sensitivity of the network modules to quantization. As a final note, CA-SpaceNet does not quantize the first and last layer in any quantization mode. In contrast, MQ quantizes the entire network.

Finally, we evaluate MQ on a multi-stage network architecture. Specifically, in Table 7, we demonstrate the performance of our method on the current best performing 6D pose estimation network, the two-stage ZebraPose network [38]. The results evidence that Module-wise Quantization (MQ) outperforms the state-of-the-art HAWQv3 [47] by  $\sim 1.3\%$ , while even compressing the network slightly more. We did not observe an improvement over the full precision performance; this was only observed with single-stage network architectures containing an FPN.

## 5. Limitations

*Quantization Flow.* As conclusively demonstrated in Section 4.2.1, MQ exploits the modular format of a network in a systematic way. If the network does not contain distinct modules, MQ simply converges to a uniform QAT

Quantization Mode	ADI-0.1d	Compression
Full precision	76.90	1x
HAWQv3 (Uniform) [47]	69.87	4x
HAWQv3 (Mixed-Precision) [47]	71.11	4.60x
<b>MQ (ours)</b>	<b>72.38</b>	<b>4.62x</b>

Table 7. **Quantization of ZebraPose [41]**. We report ADI scores on the O-LINEMOD dataset.

methodology. In principle, MQ can apply to any architectures with  $K \geq 2$ . As shown in Algorithm 1, MQ currently performs a form of grid search to determine the optimal bit-precision for each module. This is manageable for a  $K = 3$  module network, but quickly becomes lengthy for networks with more modules. In future work, we intend to provide a procedure that will inform an optimal bit-precision based on module sensitivity and network compression requirements, without requiring a grid search.

*Latency.* Directly reporting latency measurements involves hardware deployment, which goes beyond the scope of this work. However, as shown in [47], latency is directly related to the bit operations per second (BOPs). With lower-precision networks, both the model size and the BOPs are reduced by the same compression factor, which we provide in our experiments. Therefore, it is expected that MQ would demonstrate a latency improvement proportional to the network compression factor and consequent reduction in BOPs.

## 6. Conclusion

We have introduced a Module-wise Quantization (MQ) strategy for networks that exhibit a modular structure, such as 6D object pose estimation architectures. Our approach builds on the intuition that the individual modules of such networks are unique, and thus should be quantized uniquely while heeding an optimal quantization order. Our extensive experiments on different datasets and network architectures, and in conjunction with different quantization methods, conclusively demonstrate that MQ outperforms uniform and mixed-precision quantization methods at various compression factors. Moreover, we have shown that it can even enhance network performance. In particular, aggressive quantization of the network FPN resulted in 7.8% and 2.4% test set accuracy improvements over the full-precision network on LINEMOD and O-LINEMOD, respectively. In the future, we will investigate the applicability of MQ to tasks other than 6D object pose estimation. We also intend to replace the current grid search for bit-width precision with an automated solution based on the modules’ sensitivities.



## References

- [1] Yash Bhalgat, Jinwon Lee, Markus Nagel, Tijmen Blankevoort, and Nojun Kwak. LSQ+: Improving low-bit quantization through learnable offsets and better initialization. *In Proceedings of the IEEE/CVF Computer Vision and Pattern Recognition*, 2020. 2, 3
- [2] David Blalock, Jose Javier, Gonzalex Ortiz, Jonathan Frankle, and John Gutta. What is the State of Neural Network Pruning? *In Proceedings of the Machine Learning and Systems*, 2020. 2
- [3] Eric Brachmann, Alexander Krull, Frank Michel, Stefan Gumhold, Jamie Shotton, and Carsten Rother. Learning 6D Object Pose Estimation using 3D Object Coordinates. *In Proceedings of the IEEE/CVF European Conference on Computer Vision*, 2014. 2
- [4] Yaohui Cai, Zhewei Yao, Zhen Dong, Amir Gholami, Michael W Mahoney, and Kurt Keutzer. Zeroq: A novel zero shot quantization framework. *In Proceedings of the IEEE/CVF Conference on Computer Vision and Pattern Recognition*, 2020. 2
- [5] Zhaowei Cai and Nuno Vasconcelos. Rethinking Differentiable Search for Mixed-Precision Neural Networks. *In Proceedings of the IEEE/CVF Computer Vision and Pattern Recognition*, 2020. 1, 2, 3
- [6] Bo Chen, Jiewei Cao, Álvaro Parra, and Tat-Jun Chin. Satellite Pose Estimation with Deep Landmark Regression and Nonlinear Pose Refinement. *In Proceedings of the IEEE/CVF International Conference on Computer Vision Workshop*, 2019. 1, 2, 7
- [7] Peng Chen, Jing Liu, Bohan Zhuang, Minghui Tan, and Chunhua Shen. AQD: Towards Accurate Quantized Object Detection. *In Proceedings of the IEEE/CVF Computer Vision and Pattern Recognition*, 2021. 2
- [8] Wei Han Chen, Peisong Wang, and Jian Cheng. Towards Mixed-Precision Quantization of Neural Networks via Constrained Optimization. *In Proceedings of the IEEE/CVF International Conference on Computer Vision*, 2021. 3
- [9] Yan Di, Fabian Manhardt, Gu Wang, Xiangyang Ji, Nassir Navab, and Federico Tombari. SO-Pose: Exploiting Self-Occulsion for Direct 6D Pose Estimation. *In Proceedings of the IEEE/CVF International Conference on Computer Vision*, 2021. 1, 2, 3, 5
- [10] Zhen Dong, Zhewei Yao, Yaohui Cai, Daiyaan Arfeen, Amir Gholami, Michael W. Mahoney, and Kurt Keutzer. HAWQ-V2: Hessian Aware trace-Weighted Quantization of Neural Networks. *In Proceedings of the Neural Information Processing Systems*, 2020. 1, 2, 3
- [11] Zhen Dong, Zhewei Yao, Amir Gholami, Michael Mahoney, and Kurt Keutzer. HAWQ: Hessian AWARE Quantization of Neural Networks with Mixed-Precision. *In Proceedings of the IEEE/CVF International Conference on Computer Vision*, 2019. 2, 3
- [12] Steven K. Esser, Jeffrey L. McKinstry, Deepika Bablani, Rathinakuma Appuswamy, and Dharmendra S. Modha. Learned Step Size Quantization. *In Proceedings of the International Conference on Learning Representations*, 2020. 2, 3, 5, 7
- [13] Elias Frantar and Dan Alistarh. Optimal Brain Compression: A Framework for Accurate Post-Training Quantization and Pruning, 2022. 2
- [14] Stefan Hinterstoisser, Vincent Lepetit, Slobodan Ilic, Stefan Holzer, Gary R. Bradski, Kurt Konolige, and Nassir Navab. Model Based Training, Detection and Pose Estimation of Texture-Less 3D Objects in Heavily Cluttered Scenes. *In Proceedings of the Asian Conference on Computer Vision*, 2012. 2
- [15] Tomáš Hodaň, Dániel Baráth, and Jiří Matas. EPOS: Estimating 6D pose of objects with symmetries. *In Proceedings of the IEEE/CVF Computer Vision and Pattern Recognition*, 2020. 1
- [16] Tomáš Hodaň, Jiří Matas, and Štěpán Obdržálek. On Evaluation of 6D Object Pose Estimation. *In Proceedings of the European Conference on Computer Vision Workshops*, 2016. 5
- [17] Yinlin Hu, Joachim Hugonot, Pascal Fua, and Mathieu Salzmann. Segmentation-Driven 6D Object Pose Estimation. *In Proceedings of the IEEE/CVF Computer Vision and Pattern Recognition*, 2019. 2, 7
- [18] Yinlin Hu, Sébastien Speierer, Wenzel Jakob, Pascal Fua, and Mathieu Salzmann. Wide-Depth-Range 6D Object Pose Estimation in Space. *In Proceedings of the IEEE/CVF Computer Vision and Pattern Recognition*, 2021. 1, 2, 3, 5, 6, 7
- [19] Shun Iwase, Xingyu Liu, Rawal Khrodar, Rio Yokota, and Kris M. Kitani. RePOSE: Fast 6D Object Pose Refinement via Deep Texture Rendering. *In Proceedings of the IEEE/CVF International Conference on Computer Vision*, 2021. 2
- [20] Omid Hosseini Jafari, Siva Karthik Mustikovela, Karl Pertsch, Eric Brachmann, and Carsten Rother. iPose: Instance-Aware 6D Pose Estimation of Partly Occluded Objects. *In Proceedings of the Asian Conference on Computer Vision*, 2018. 2
- [21] W. Kehl, F. Manhardt, F. Tombari, S. Ilic, and N. Navab. SSD-6D: Making RGB-Based 3D Detection and 6D Pose Estimation Great Again. *In Proceedings of the IEEE/CVF International Conference on Computer Vision*, 2017. 2
- [22] Yann Labbé, Justin Carpentier, Mathieu Aubry, and Josef Sivic. CosyPose: Consistent multi-view multi-object 6D pose estimation. *In Proceedings of the European Conference on Computer Vision*, 2020. 2, 3, 7
- [23] Yuhang Li, Ruihao Gong, Zu Tan, Yang Yang, Peng Hu, Qi Zhang, Fengwei Yu, Wei Wang, and Shi Gu. BRECCQ: Pushing the Limit of Post-Training Quantization by Block Reconstruction. *In Proceedings of the International Conference on Learning Representations*, 2021. 2
- [24] Zhigang Li, Gu Wang, and Xiangyang Ji. CDPN: Coordinates-Based Disentangled Pose Network for Real-Time RGB-Based 6-DoF Object Pose Estimation. *In Proceedings of the IEEE/CVF International Conference on Computer Vision*, 2019. 2, 3
- [25] Tsung-Yi Lin, Piotr Dollár, Ross Girshick, Kaiming He, Bharath Hariharan, and Serge Belongie. Feature Pyramid Networks for Object Detection. *In Proceedings of the*

- IEEE/CVF Computer Vision and Pattern Recognition*, 2016. 2
- [26] Wei Liu, Dragomir Anguelov, Dumitru Erhan, Christian Szegedy, Scott E. Reed, Cheng-Yang Fu, and Alexander C. Berg. SSD: Single Shot MultiBox Detector. *In Proceedings of the European Conference on Computer Vision*, 2016. 2
  - [27] Markus Nagel, Rana Ali Amjad, Mart van Baalen, Christos Louizos, and Tijmen Blanevoort. Up or Down? Adaptive Rounding for Post-Training Quantization. *In Proceedings of the International Conference on Machine Learning*, 2020. 2
  - [28] Markus Nagel, Mart van Baalen, Tijmen Blankevoort, and Max Welling. Data-Free Quantization Through Weight Equalization and Bias Correction. *In Proceedings of the IEEE/CVF International Conference on Computer Vision*, 2019. 2
  - [29] M. Oberweger, M. Rad, and V. Lepetit. Making Deep Heatmaps Robust to Partial Occlusions for 3D Object Pose Estimation. *In Proceedings of the European Conference on Computer Vision*, 2018. 2
  - [30] Sida Peng, Yuan Liu, Qixing Huang, Hujun Bao, and Xiaowei Zhou. PVNet: Pixel-wise Voting Network for 6DoF Pose Estimation. *In Proceedings of the IEEE/CVF Computer Vision and Pattern Recognition*, 2019. 1, 2, 3, 5, 7
  - [31] Luis Pérez, Ínigo Rodríguez, Nuria Rodríguez, Rubén Usamentiaga, and Daniel F. García. Robot Guidance Using Machine Vision Techniques in Industrial Environments: A Comparative Review. *Sensors*, 2016. 1
  - [32] Julien Posso, Guy Bois, and Yvon Savaria. Mobile-URSONet: an Embeddable Neural Network for Onboard Spacecraft Pose Estimation. *In Proceedings of the IEEE International Symposium on Circuits and Systems*, 2022. 2
  - [33] Pedro F. Proença and Yang Gao. Deep Learning for Spacecraft Pose Estimation from Photorealistic Rendering. *In Proceedings of the IEEE International Conference on Robotics and Automation*, 2020. 2
  - [34] Mahdi Rad and Vincent Lepetit. BB8: A Scalable, Accurate, Robust to Partial Occlusion Method for Predicting the 3D Poses of Challenging Objects without Using Depth. *In Proceedings of the IEEE/CVF International Conference on Computer Vision*, 2017. 1, 2
  - [35] Abhilasha Singh, V. Kalaichelvi, and R. Karthikeyan. A survey on vision guided robotic systems with intelligent control strategies for autonomous tasks. *Cogent Engineering*, 2022. 1
  - [36] Chen Song, Jiaru Song, and Qixing Huang. HybridPose: 6D Object Pose Estimation under Hybrid Representations. *In Proceedings of the IEEE/CVF Computer Vision and Pattern Recognition*, 2020. 1
  - [37] Jianing Song, Duarte Ronda, and Nabil Aouf. Deep learning-based spacecraft relative navigation methods: A survey. *In Proceedings of the Acta Astronautica*, 2022. 1
  - [38] Yongzhi Su, Mahdi Saleh, Torben Fetzner, Jason Rambach, Nassir Navab, Benjamin Busam, Didier Stricker, and Federico Tombari. ZebraPose: Coarse to Fine Surface Encoding for 6DoF Object Pose Estimation. *In Proceedings of the IEEE/CVF Computer Vision and Pattern Recognition*, 2022. 1, 2, 3, 5, 7, 8
  - [39] Chen Tang, Kai Ouyang, Zhi Wang, Yifei Zhu, Yaowei Wang, Wen Ji, and Wenwu Zhu. Mixed-Precision Neural Network Quantization via Learned Layer-wise Importance. *In Proceedings of the European Conference on Computer Vision*, 2022. 1, 2, 3
  - [40] Bugra Tekin, Sudipta N. Sinha, and Pascal Fua. Real-Time Seamless Single Shot 6D Object Pose Prediction. *In Proceedings of the IEEE/CVF Computer Vision and Pattern Recognition*, 2018. 2, 3
  - [41] Stefan Thalhammer, Markus Leitner, Timothy Patten, and Markus Vincze. PyraPose: Feature Pyramids for Fast and Accurate Object Pose Estimation under Domain Shift. *In Proceedings of the IEEE International Conference on Robotics and Automation*, 2021. 1, 2, 3, 7
  - [42] F. Vicentini. Collaborative Robotics: A Survey. *American Society of Mechanical Engineers, J. Mech. Design*, 2021. 1
  - [43] Gu Wang, Favian Manhardt, Federico Tombari, and Xiangyang Ji. GDR-Net: Geometry-Guided Direct Regression Networks for Monocular 6D Pose Estimation. *In Proceedings of the IEEE/CVF Computer Vision and Pattern Recognition*, 2021. 1, 2, 3, 5, 7
  - [44] Shunli Wang, Shuaibing Wang, Bo Jiao, Dingkan Yang, Liuzhen Su, Peng Zhai, Chixiao Chen, and Lihua Zhang. CA-SpaceNet: Counterfactual Analysis for 6D Pose Estimation in Space. *In Proceedings of the IEEE/RSJ International Conference on Intelligent Robots and Systems*, 2022. 1, 2, 3, 5, 6, 7, 8
  - [45] Yu Xiang, Tanner Schmidt, Venkatraman Narayanan, and Dieter Fox. PoseCNN: A Convolutional Neural Network for 6D Object Pose Estimation in Cluttered Scenes. *In Proceedings of the Robotics: Science and Systems (RSS)*, 2018. 2
  - [46] Kohei Yamamoto. Learnable Companding Quantization for Accurate Low-bit Neural Networks. *In Proceedings of the IEEE/CVF Computer Vision and Pattern Recognition*, 2021. 2, 3
  - [47] Zhewei Yao, Zhen Dong, Zhangcheng Zheng, Amir Gholami, Jiali Yu, Eric Tan, Leyuan Wang, Qijing Huang, Yida Wang, Michael W. Mahoney, and Kurt Keutzer. HAWQV3: Dyadic Neural Network Quantization. *In Proceedings of the International Conference on Machine Learning*, 2020. 2, 3, 7, 8
  - [48] Sergey Zakharov, Ivan Shugurov, and Slobodan Ilic. DPOD: 6D Pose Object Detector and Refiner. *In Proceedings of the IEEE/CVF International Conference on Computer Vision*, 2019. 2
  - [49] Ritchie Zhao, Yuwei Hu, Jordan Dotzel, Chris De Sa, and Zhiru Zhang. Improving Neural Network Quantization without Retraining using Outlier Channel Splitting. *In Proceedings of the International Conference on Machine Learning*, 2019. 2
  - [50] Aojun Zhou, Anbang Yao, Yiwen Guo, Lin Xu, and Yurong Chen. Incremental Network Quantization: Towards Lossless CNNs with Low-Precision Weights. *In Proceedings of the International Conference on Learning Representations*, 2017. 2, 3, 5, 7